# Anchoring nano-zeolite NaX particles on polydopamine-modified PVDF/PAN electrospun membranes for enhancing interception, adsorption and antifouling performance

Wenyan He, Mi Zhang, Huiling Du, Abdeltif Amrane, Haiyan Yu, Yihang Liu

# Anchoring nano-zeolite NaX particles on polydopamine-modified PVDF/PAN electrospun membranes for enhancing interception, adsorption and antifouling performance

Wenyan He[1,*], Mi Zhang[1], Huiling Du[2], Abdeltif Amrane[3], Haiyan Yu[1], Yihang Liu[1]

1. College of Geology and Environment, Xi'an University of Science and Technology, Xi' an 710054, PR China
2. College of Materials Science and Engineering, Xi'an University of Science and Technology, Xi' an 710054, PR China
3. École Nationale Supérieure de Chimie de Rennes, CNRS, ISCR (Institut des Sciences Chimiques de Rennes)–UMR 6226, Université Rennes, F-35000 Rennes, France

## Abstract

In this study, hydrophilic nano-zeolite NaX particles were successfully grafted onto poly(vinylidene fluoride)/polyacrylonitrile (PVDF/PAN) membrane through PDA (polydopamine) blending and coating techniques. The preparation parameters of PDA-blended or coated membranes on the chemical oxygen demand (COD) removal efficiency and solution flux were systematically investigated. Subsequently, the "bio-glue" of PDA made the nano-zeolite NaX particles anchor successfully onto its modified PVDF/PAN membranes through two methods. The selected M2' membrane, obtained via in situ nano-zeolite NaX loading, exhibited exceptional bovine serum

albumin (BSA) concentration efficiency (93.75%), outstanding $NH_4^+$ removal efficiency (98%), high flux (198 L/($m^2$·h)), and remarkable hydrophilicity due to the synergistic effect of PDA and nano-zeolite. The adsorption kinetics of $NH_4^+$ on all nano-zeolite NaX-modified membranes fitted well with the Avrami fractional-order (AFO) model. After modification by PDA and nano-zeolite NaX, M2 and M2' showed excellent antifouling performance because of the enhanced hydrophilicity, and the forceful electrostatic repulsion with BSA contaminant. Compared to M2, M2' displayed more stable and efficient filtration performance even after multiple cycles of simple regeneration. This study provides a practical and viable approach for the implementation of environmentally friendly adsorption/separation membranes in organic carbon interception and ammonium recovery.

**Keywords:** Ammonium; Bovine serum albumin; PDA; Electrospun fiber membrane modification;

## Introduction

Nowadays, the world is facing many disastrous problems such as severe water shortages, energy shortages, and resource depletion [1, 2], which endanger the sustainable development of human society. Municipal sewage treatment is closely related to these fatal issues. The defects of “energy consumption” and neglect of resource circulation in traditional sewage treatment are more evident [3]. Therefore, sustainable water treatment technology, which regards sewage as a resource and energy carrier, has gradually attracted widespread attention [4, 5]. In urban sewage treatment technology, efficient resource recovery and utilization of water resources,

organic energy, and nutrient elements (nitrogen and phosphorus) should be pursued [6, 7]. The electrospun fiber membrane separation technique has been proven to be an effective and promising route for water filtration due to its high porosity and large surface area to volume ratio, resulting in high permeability and filtration efficiency [2, 8-10]. In addition, modifying the surface of the electrospinning fiber membrane to obtain multifunctional membranes could be more widely applied in wastewater treatment [2, 9, 11-13].

Even though the average concentration of chemical oxygen demand (COD) and ammonia nitrogen in municipal sewage is relatively low, due to the large water volume based, a mass of nutrients could be recycled. According to the China Water Resources Bulletin, 57.1 billion M2 of municipal sewage was discharged in 2020, with COD and ammonia nitrogen levels of 25.121 million tons and 0.961 tons, respectively. Directly discharging such a large amount of pollutants into rivers would cause permanent harm to aquatic organisms and even the water ecosystem [14, 15]. Yu et al. [16] have demonstrated that nitrogen pollution in China's environmental water bodies has exceeded the "safe" limit, and the rate of man-made nitrogen entering the water body is almost three times higher than that of the "safe" level estimate. Efficient recovery and reuse of these resources could provide new solutions to transform municipal sewage treatment plants from "energy consumption" to "production capacity" [17]. Therefore, the efficient recovery of low-concentration organic carbon sources and ammonia nitrogen in municipal wastewater has dual significance for solving the energy and resource crisis.

Nano-particles and zeolite-like metal-organic frameworks (MOF) based pressure-driven composite membrane materials have been widely studied in the field of water resource recycling [18]. Our previous study has demonstrated that nano-zeolite NaX with a faujasite-type structure and low Si/Al atomic ratio of 1.4, exhibited the best ammonium adsorption efficiency than that of nano-zeolite NaA, sodalite, nano-zeolite NaY, clinoptilolite, modified clinoptilolite (treated with NaOH), zeolite Na-P1, multiphase zeolite (zeolite X, zeolite A, zeolite P, and hydroxysodalite), due to the cooperative effects of adsorption, ion-exchange and a large amount of weak acid sites mechanism [19]. In addition, the regenerated nano-zeolite NaX still maintained about 93% ammonium removal efficiency after five regeneration cycles. Based on the excellent, stable, and efficient adsorption efficiency of nano-zeolite NaX toward ammonium removal, it was chosen to modify electrospun membranes (EMs) to concurrently enrich organic materials and recover ammonium [5]. However, to expose more of the nano-zeolite NaX particles, which were coated by the hydrophobic polymer layer, the dissolution of the pore-forming agent PVP harmed the structural soundness of the membranes. Therefore, it has become urgently necessary to find a solution to load nano-zeolite particles equally on the fiber's surface without affecting the integrity of the membrane and avoiding zeolite particles from being encapsulated by the polymer film. Deng et al. [20] proved that the core-shell structure was achieved by the coaxial electrospinning technology, which allows $\gamma$-$Fe_2O_3$ nanoparticles to be loaded on mineral oil in the form of tube walls. However, it is difficult to find a suitable solvent that does not encapsulate zeolite nanoparticles but

can be used in electrospinning. Attempts such as chemical modification and self-assembly strategies in composite electrospun membranes were performed to solve the aforementioned problems. Moradi and Zinadini [10] demonstrated that with the aid of the functional carboxylate and citrate alumoxane groups, the hyper-branched polycitrate-para-aminobenzoate alumoxane was successfully loaded on PAN microfiltration membranes. However, due to the weak binding force, this approach is hard to modify PVDF membranes with nano-zeolites. Numerous studies have confirmed that a lack of thermodynamic compatibility between inorganic substance and organic polymer causes defects and reduced strength of the composite materials [18, 21].

Polydopamine, obtained via the self-polymerization of dopamine, has attracted a great deal of attention in the modification of material surfaces because of not only its extraordinary surface functional groups (-OH, $-NH_2$) but also its substrate-independent coating ability [9, 22, 23]. Mavukkandy et al. [2] proved that after the surface of poly(vinylidene fluoride-co-hexafluoropropylene) was coated with PDA, the $WO_3$ nanoparticles could be incorporated into the top layers. Gao et al. [24] utilized PDA as an adhesive to intensify the bond between silver nanoparticles and cotton fibers, and thus to obtain flexible and wearable cotton fabrics with ultra-high superhydrophobic properties. Additionally, $TiO_2$ particles were successfully loaded on the hydrophobic PVDF membranes with the help of PDA, so their hydrophilicity, stability, and antifouling properties were all significantly improved [25]. Moreover, PDA also promoted the mechanical strength of the fiber composite materials while

retaining their porous structure and high water permeability [8, 12]. Therefore, the typical flux loss caused by the aggregation of nanoparticles clogging membrane pores could be mitigated. In another way, PDA could also be blended by adding DA in the precursor solution, and then self-polymerization of DA was induced to obtain PDA-modified fiber membranes. And the enhanced hydrophilicity and excellent adsorption ability to methylene blue and $Cu^{2+}$ were due to the formation of PDA-blended layers [9]. However, to the best of our knowledge, no studies have been conducted to compare the effects of different loading methods of PDA on the performance of nano-zeolite NaX-modified composite electrospun fiber membranes. In addition, the thermodynamic compatibility of blends of PDA and PVDF/PAN also needs to be investigated based on similar reports [26-29].

In this study, PDA-coated or blended PVDF/PAN EMs were prepared and then have been post-modified by nano-zeolite NaX in two ways. Due to the tight binding force of the PDA layer, nano-zeolite NaX particles could be uniformly built on the surface of PVDF/PAN EMs without destroying the skeleton structures of membranes. The obtained multifunctional composite membranes were physicochemically characterized in detail, and the solution flux, BSA rejection, and ammonium adsorption properties have been thoroughly investigated and compared. Moreover, ammonium adsorption kinetics and reusability of the nano-zeolite NaX-modified PDA blended and coated membranes have been experimentally examined. And the effect of PDA and nano-zeolite NaX on the antifouling performance of the membrane was also investigated. Our study proposed a reasonable and efficient strategy for carbon source

concentration and ammonia nitrogen recovery from municipal wastewater using composite electrospun membranes obtained in a simple process.

## 2. Experimental methods

### 2.1 Materials

The nano-zeolite NaX was fabricated according to the literature [19]. Typically, 16.54 g of sodium hydroxide was dissolved in 157.5 g of deionized water, then 7.53 g of sodium aluminate was dissolved in half of the obtained solution, and 11.02 g of fumed silica was dissolved in the other half at 100 °C. After the solution cooled to 5°C, the silicate solution was added dropwise into the aluminate solution with vigorous stirring. Thereafter, the mixed solution was transferred to a polytetrafluoroethylene bottle and put in an oven at 60 °C for 48 hours. The product centrifugated at 14000 rpm for 30 min and washed several times with distilled water until the pH value of the solution was nearly 8.0. Finally, it was dried at 60 °C overnight.

PVDF (Mw≈317100) was purchased from Beijing Yongkang Leye Technology Development Co., Ltd. PAN (Mw=150000), dopamine hydrochloride (98%), and Tris-HCl buffer (1.0 M, pH=8.5) were all obtained from Macklin. BSA was purchased from Shanghai Ruji Biological Technology Development Co., Ltd. COD reagent was obtained from Beijing Lianhua YongXing Science and Technology Development Co., Ltd. Ammonium chloride was obtained from Tianjin Kemiou Chemical Reagent Co., Ltd. Analytic reagents of N, N-dimethylformamide (DMF) and acetone were obtained from Tianjin Fuyu Fine Chemical Co., Ltd. All solutions

were prepared with ultrapure water by using Milli Q purification system at 18.2 MΩ cm.

**2.2 Preparation of PDA-modified composite EMs**

Preparation of PDA blended-PVDF/PAN (M1') EMs. The fabrication protocols of DA blended-PVDF/PAN (M0) composite EMs were modified from literature conditions [9]. 10% PVDF, 0-2% PAN, and 0-7% DA were dissolved in the mixed solution of DMF/acetone (3:7, v:v) at 80°C and stirred vigorously for 10 min. Then the EMs were fabricated with automatic electrospinning equipment (Dalian Dingtong Technology Development Co., Ltd.). The voltage was 20±1.5 kV and the speed of the injection pump was 0.01 μL/min. An aluminum foil connected to a counter electrode was used to collect the mat with a rotating speed of 100 r/min, which was 10 cm apart from the spinneret with a 21-gauge needle. The ambient temperature was 25-30 $^{o}$C, and humidity was 30%-40%. The obtained PVDF/PAN (PP, without DA) or M0 electrospun mats were dried in an oven at 60 °C for 18 h. To increase the interception efficiency of membranes, part of the obtained electrospun mats were hot-pressed at 180 °C, 10 MPa for 3 minutes, and was named PP-H and M0', respectively. After that, M0' was dipped into Tris-HCl solution (1.0 M, pH=8.5, 30℃) for 0-42 h to induce the self-polymerization of dopamine to obtain M1'. And then it was carefully washed with deionized water to remove the residual Tris-HCl solution, and dried in an oven at 60 °C for 5 h.

Preparation of PDA coated-PVDF/PAN (M1) EMs. The selected PP-H electrospun membrane, which had the best BSA rejection and solution flux was firstly

dipped into the Tris-HCl solution (1.0 M, pH=8.5, 30℃) for 5 min, and then it was put into the DA solution (0-4 mg/mL) and oscillated in a water bath thermostat at 25 $^{o}$C for 2 h. The following protocols were the same as the M1' EMs. Repeated the above experimental procedure 2-6 times to get the M1 with the best BSA rejection and solution flux.

**2.3 Preparation of the nano-zeolite NaX-modified composite electrospun fiber membranes**

As shown in Fig.1, the nano-zeolite NaX particles were doped in situ on the selected M1' and M1 electrospun membranes by hydrothermal reaction under the same conditions as nano-zeolite NaX preparation, named M2' and M2, respectively [19]. For comparison, the selected M1' and M1 electrospun membranes were immersed into the aqueous solution of nano-zeolite NaX (594 mg/L) at 60 $^{o}$C for 48 h to obtain M3' and M3. Besides, to verify the adhesion of the PDA to nano-zeolite NaX, PP-H-Z (without PDA coating) and M0'-Z (without inducing DA self-polymerization) were also prepared under the same conditions as M2 and M2'.

All details of the electrospun fiber membranes prepared in this study, including the names and compositions were presented in Table S1.

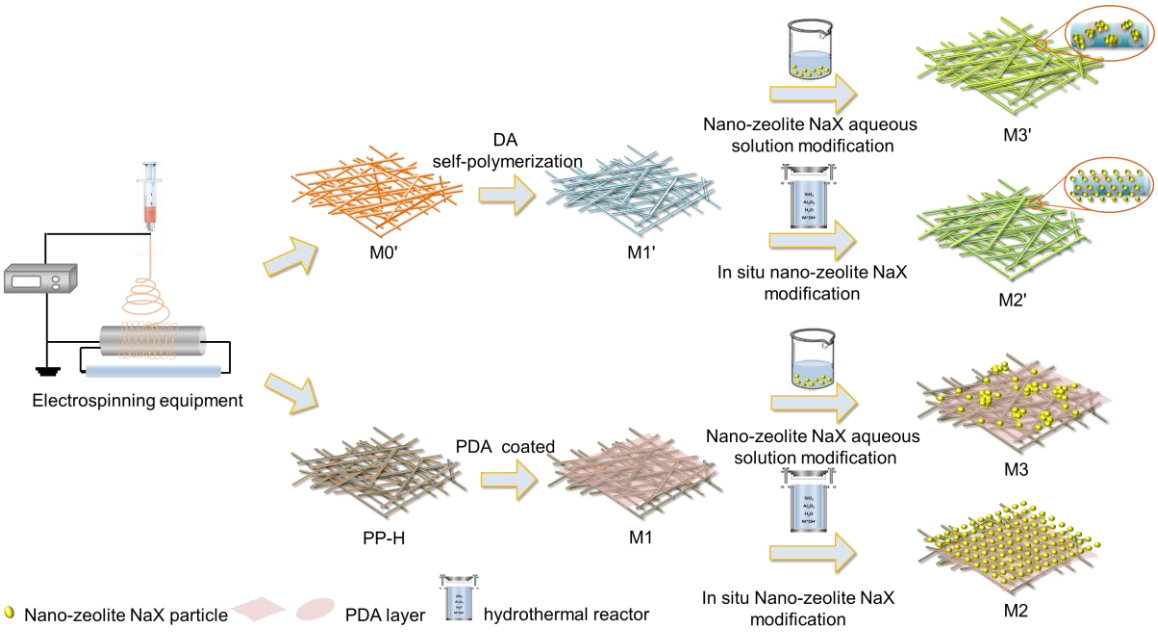


Fig.1 Schematic diagram of the preparation process of PDA and nano-zeolite NaX modified EMs.

**2.4 Characterization of the prepared composites electrospun fiber membranes**

The surface morphologies of the obtained membranes were observed by field emission scanning electron microscopy (JSM-7610F, Electronics Co., Ltd, Japan). The roughness of the membrane surface was investigated by three-dimensional atomic force microscope (AFM, Dimension, German) with surface roughness ($R_a$) and root roughness ($R_q$). The hydrophilicity of the membranes was evaluated by testing the water contact angles with a drop-shape analyzer (OCA25, Dataphysics Instruments Co., Ltd, Germany) at three different locations. Zeta potentials were measured by a zeta potentiometer (Nano-ZS90, Malvin Instruments, Ltd, UK). The mean pore size of the selected membranes was tested by a capillary flow porometer (CFP, porolux1000, IB-FT, Germany). Mechanical properties of the PP, M0, M2 and M2' electrospun membranes were measured based on the literature [5]. To confirm whether the PDA was successfully loaded on the membranes, Attenuated Total Reflectance-Fourier

Transform Infrared (ATR-FTIR) spectroscopy (Tensor II, Bruker Corporation, Germany) measurements were performed.

**2.5 Filtration and adsorption performance test**

A dead-end ultrafiltration cell (50 mL, Model 8200, Millipore, USA), which was equipped with nitrogen pressure control, was used for filtration and dynamic adsorption experiments. The simulated wastewater containing bovine serum albumin (COD: 250 mg/L and ammonium (20 mg N/L) was applied to test the ammonium and BSA rejection performance of the M2, M2', M3 and M3' electrospun fiber membranes at 40 kPa. The samples were taken every 2 minutes, the concentration of COD was measured by the potassium dichromate method and analyzed by a COD meter (5B-3A, Beijing Lianhua Yongxing Technology Development Co., Ltd, China). Detailed information was in the Supplementary file. The BSA rejection of the membranes was measured by calculating its COD retention rate, which is defined as:

$$\text{BSA rejection}\% = \frac{COD_0 - COD_t}{COD_0} \times 100\% \quad (1)$$

where, $COD_0$ is the concentration of COD of the initial solution, and $COD_t$ is the concentration of COD of the permeate.

Ammonium concentration was measured by Nessler's reagent spectrophotometric method and the absorbance was analyzed by a spectrophotometer (Inesa-L5S, Shanghai Yidian Scientific Instrument Co., LTD., China). The reusability of the membranes was performed by using the sodium chloride solution in an ultrasound bath for regeneration [5]. The static adsorption of ammonium protocols and kinetic models were in SI.

**2.6 Analysis of the antifouling performance of the membrane**

To illustrate the enhanced combination effect of PDA and nano-zeolite NaX on the antifouling performance of the PVDF/PAN membrane, the protocols were improved according to the literature conditions [30, 31]. All experiments were performed at feed pressures of 40 kPa at 25℃. Pure water flux was recorded every 2 min, and the mean value was $J_{W1}$. And then the pure water was replaced by 250 mg/L BSA solution and filtrated for 70 min (five times, and 14 min for each filtration), and the flux was named $J_p$. After that, the membrane was washed in a thermostatic water oscillator for 30 min, and then the water flux of the washed membrane was measured again, namely, $J_{W2}$.

Actual fluxes were calculated by Eq.2.

$$J = \frac{V}{A \times t} \tag{2}$$

where, J was the actual flux (L/($m^2$·h)); V was the filtration volume (L); A was the effective membrane area ($m^2$); t was the filter interval (h).

The relevant parameters to evaluate the antifouling performance of the membranes, such as flux recovery ratio (FRR), reversible resistance ratio [11] [11], and irreversible resistance ratio ($R_{ir}$) were as follows [25]:

$$FRR = \frac{J_{W2}}{J_{W1}} \times 100\ \% \tag{3}$$

$$R_r = \left( \frac{J_{W2} - J_P}{J_{W1}} \right) \times 100\ \% \tag{4}$$

$$R_{ir} = \left( \frac{J_{W1} - J_{W2}}{J_{W1}} \right) \times 100\% \tag{5}$$

where, $J_{W1}$, $J_p$, and $J_{W2}$ were the mean flux of pure water, the BSA solution, and the washed membrane, respectively.

## 3. Results and Discussion

### 3.1 Characterization of the prepared electrospun fiber membranes

Fig.2 exhibits the ATR-FTIR spectra of the composite electrospun fiber membranes before and after PDA coating or blending. Compared to PP and PP-H, new absorption peaks appeared at 1600 $cm^{-1}$ and 1506 $cm^{-1}$ for M1 (Fig.2a), which ascribed to the C=C resonance vibrations in the aromatic ring and the N-H bending vibrations, respectively [23, 25]. However, no PDA signal peaks were observed in M0 probably because it contained only DA monomers. And the same peaks were raised in M1' as in M1 after DA self-polymerization, which confirmed the successful formation of the PDA layers on two kinds of composite membranes surface. Different from M2 and M3, the peak of C=C resonance vibrations of M2' and M3' was still apparent after nano-zeolite NaX modification, this was mainly because PDA existed uniformly in the single blended fibers, rather than simply loaded on the outer surface of the membrane, which were easy to detect.

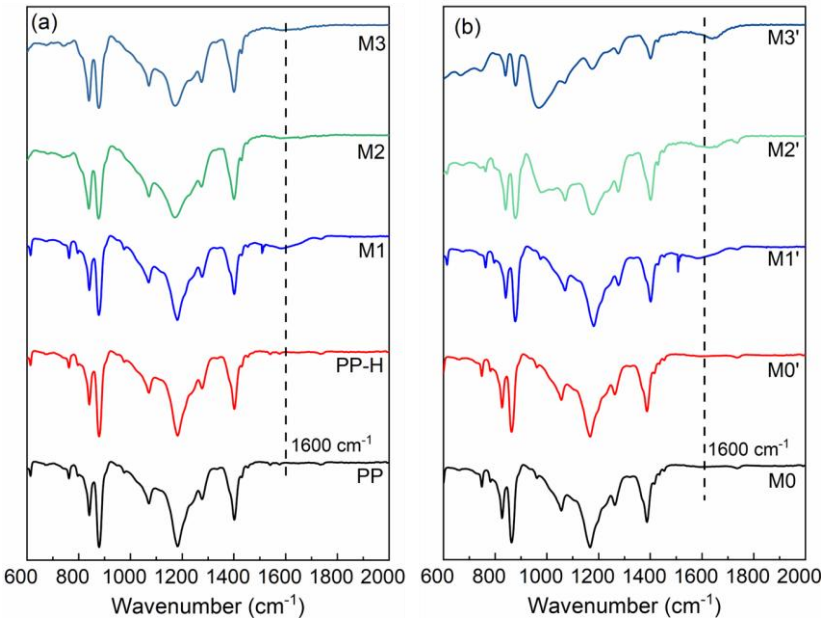


Fig.2 ATR-FTIR spectra of the composite electrospun membranes before and after (a) PDA-coating (b) or PDA-blending.

Fig.3 indicates the surface morphologies of the nano-zeolite NaX-modified electrospun fiber membranes prepared by two different PDA and nano-zeolite NaX doping methods. Compared to the relatively smooth surface of the PP, the conglutination/fusion between nanofibers of M1 was very obvious, and the formed PDA layer on the surface of the membrane was the same as the reported PDA-coated dense membranes [9, 32]. While the PDA layer was not observed on the surface of M1', the fiber diameters of M1' slightly increased, indicating that PDA was homogeneously distributed in the single fibers, which effectively promoted a decrease in the membrane aperture. As shown in Fig.4, dopamine polymerization endowed the film surface with active functional groups (hydroxyl, carbonyl, or imino groups), when the polar nano-zeolite NaX particles came into contact with the PDA-modified surface, the polarity interaction between the two formed hydrogen bonds. So that the nano-zeolite NaX particles with flower-like structures were firmly anchored on the

surface of the M2 and M2' in situ in a hydrothermal reactor (Fig.3). In addition, the tensile strength of M2 and M2' increased by 5 times and 26 times that of PP and M1', respectively, suggesting a positive role played by the PDA adhesive and hot-pressing in enhancing the mechanical properties by coating junction points throughout the membrane [8, 33]. However, for M3 and M3', the flower-shaped structures of nano-zeolite NaX particles disappeared with large particle agglomeration instead. This was because when the membranes were modified in the aqueous solution of nano-zeolite NaX particles, high temperature, and neutral conditions triggered the collapse of the nano-zeolite NaX structures, thus further leading to the decrease of ammonium adsorption efficiency.

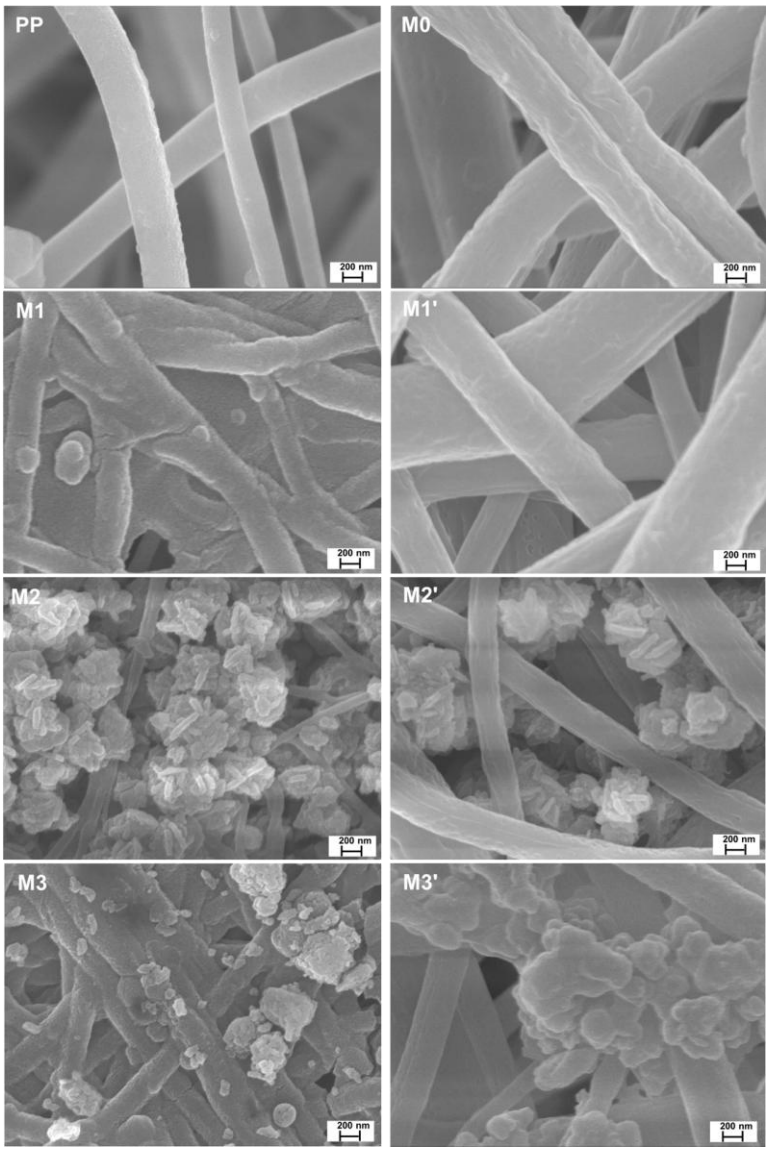


Fig.3 SEM images of the composite electrospun fiber membranes by two PDA and nano-zeolite NaX modification methods.

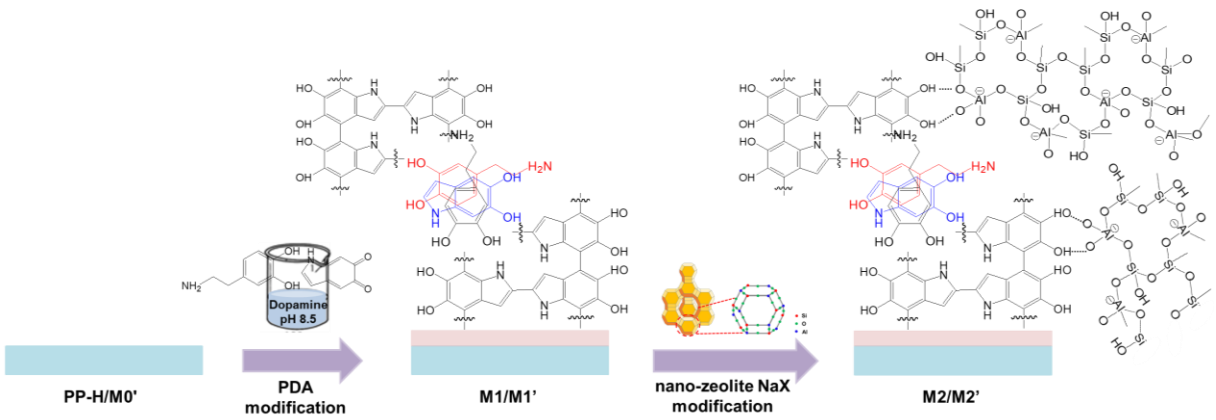


Fig.4 Bonding mechanism of nano-zeolite NaX with PDA at the interface.

As shown in Fig.5a, the water contact angle of the PP-H was almost the same as that of the PP, this means that hot-pressing cannot change the hydrophilicity of the PVDF/PAN membrane. However, it was dramatically reduced from 121.95$^{o}$ to 22.8$^{o}$ after PDA modification, and then further decreased to 15.79$^{o}$ for M2 by in situ nano-zeolite NaX modification, which was more hydrophilic than M3 (20.6$^{o}$). Different from the hydrophobic PP membrane, the M0 gave a more dramatic low water contact angle of about 18$^{o}$ due to the addition of hydrophilic DA (Fig.5b). And it became super hydrophilic after DA self-polymerization and nano-zeolite NaX modification, as the water contact angle of M2' was only 4.27$^{o}$, which was lower than that of the M3' (5.32$^{o}$). It indicated that both PDA and nano-zeolite NaX promoted the hydrophilicity of hydrophobic membranes, and PDA played a dominant role because of the presence of a large number of polar phenolic hydroxyl groups and nitrogen-containing groups in its structure [23], which were easy to have polar interactions with water molecules. Besides, compared with the nano-zeolite NaX aqueous solution loading method, the in-situ method can make more hydrophilic nano-zeolite NaX particles doped on the fiber membranes and maintaining the original structure and morphology (Fig.3), thus further improving the hydrophilicity of M2 and M2'.

Due to electrostatic attraction, the higher the negative zeta potential of the nano-zeolite NaX-modified composite EMs, the more active sites are available for ammonium adsorption [5]. As shown in Fig. 5c-5d, the zeta potential of M1 (-3.76±1.19 mV) and M1' (-3.57±0.65 mV) was almost the same as that of the primary PP membrane (-2.62±0.3 mV), indicating that PDA had little effect on improving the

zeta potential of electrospun membranes. Because PDA exhibits zwitterionic properties, which are positively charged at low pH (pH<4.7) due to the protonation of amino groups, and negatively charged at high pH (pH>4.7) because of the deprotonation of the phenolic hydroxyl groups. Nevertheless, after nano-zeolite NaX modification, the zeta potential of M2 and M2' was significantly increased to -23.3±1.3 mV and -27.03±2.1 mV, respectively, which was almost as high as that of the pure nano-zeolite NaX particles (-32.61±0.33 mV). The relatively low zeta potential of M3 (-20.18±1.16 mV) and M3' (-22.68±1.60 mV) was mainly due to their small nano-zeolite NaX load. Therefore, the effect of the loading method on the electronegativity of nano-zeolite NaX-modified fiber membranes can be ignored, indicating that there was no electrostatic interaction between nano-zeolite NaX particles and PDA-modified fiber membranes. And the hydrogen bond formed between nano-zeolite NaX and PDA structure was the main force to anchor nano-zeolite NaX particles on the membranes (Fig.4). Thus, large amounts of highly electronegative nano-zeolite NaX particles anchored on the EMs could promote the ammonium removal in the mechanism of adsorption and ion-exchange.

The CFP was used to evaluate the changes in the pore size structure of the membranes before and after modification by PDA and nano-zeolite NaX, because it significantly influenced the solution flux and BSA rejection. After hot-pressing, the average pore diameter of both PP-H and M0' was dramatically decreased to 0.35 μm (Fig. 5e-5f), which may account for the tight junctions between the fibers caused by the dissolution of PVDF at high temperatures [34]. And the pore diameters of M1 and

M1' continued to reduce after further modification by PDA. In the former, the viscous dopamine precipitated into the pores of the membrane, while in the latter, the average fiber diameter of the fibers became coarser. As we know that the smaller the membrane pore diameter, the higher the contaminant retention efficiency. Therefore, the hot-pressing and PDA coating methods were both beneficial for BSA concentration. When the membrane was modified in the aqueous solution of nano-zeolite NaX, the pore diameter of the obtained M3 and M3' remained stable. However, when the nano-zeolite was loaded in situ in a hydrothermal reactor, the pore diameters of M2 and M2' were significantly increased, this may be because alkaline solution at high temperature during the formation of nano-zeolite NaX may expand the structure of membrane pore size [35].

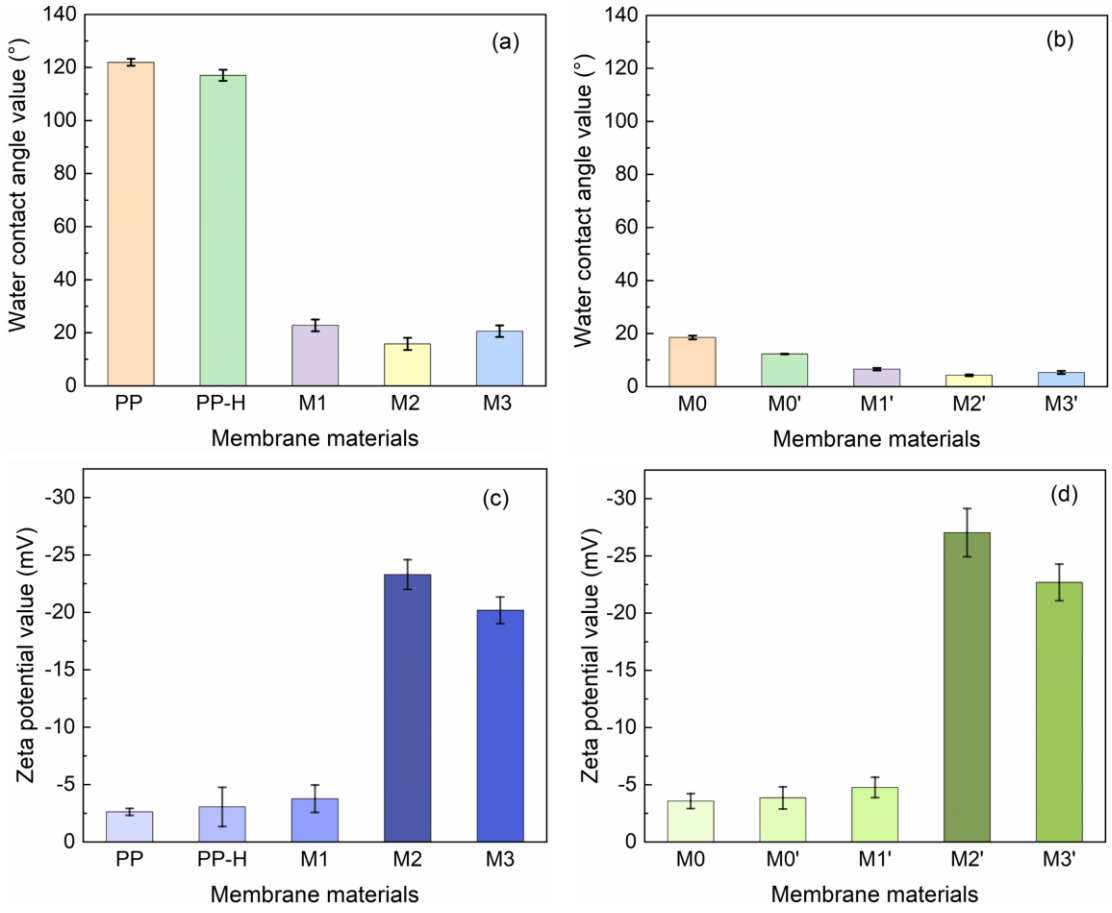

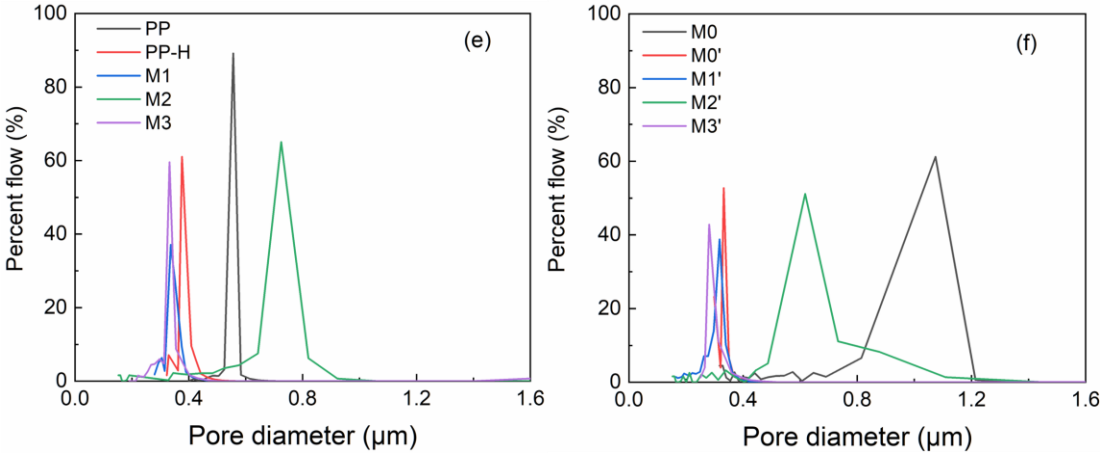


Fig.5 The water contact angles (a, b), zeta potentials (c, d), and pore diameters (e, f) of the PDA-coated composite EMs (a, c, e) and PDA-blended (b, d, f) composite EMs.

### 3.2 Optimizing the preparation conditions of M1 and M1'

Before loading nano-zeolite NaX, the preparation conditions of M1 and M1' were optimized to achieve high BSA rejection and solution flux. Fig.S1 investigated the effect of coating DA concentration, PDA coating time and its coating layers on the BSA rejection and solution flux of M1. The concentration of DA from 0 g/L to 3 g/L had limited influence on the BSA rejection (Fig.S1a), which was similar to that in Fig.S2c, indicating that the DA loading mode had little effect on the filtration performance of the membranes. The 1 hour of PDA coating time and two-tier PDA coating layers were selected because of the excellent BSA rejection (84.79±0.1%) and solution flux (240.00±0.3 L/($m^2$·h)). As shown in Fig.S2, the highest BSA rejection (210.44±1.5 L/($m^2$·h) and solution flux (88.96±0.1%) of M1' were obtained with the best ratio of 10 wt% PVDF/2 wt% PAN/3 wt% DA and 24 hours of DA self-polymerization time. The high solution flux of M1 and M1' was probably because PAN and DA can improve the porosity and hydrophilicity of the PVDF membrane, thereby reducing the water permeation resistance [9, 23, 36, 37]. Moreover, the

formed PDA layer may cover the tiny pores on the surface of the membrane, resulting in more BSA being concentrated.

### 3.3 Comparison of the filtration performance of M2 and M2' for simulated municipal wastewater

To reveal the influence of two different loading methods of PDA on nano-zeolite NaX-modified PVDF/PAN membranes, the BSA rejection, $NH_4^+$ removal efficiency, and BSA solution flux of M2, M2', M3, and M3' were performed. As shown in Fig.6a-6b, compared to PP and M0, the BSA rejection of M1 and M1' was significantly increased after hot-processing and PDA modification. There were three reasons to explain this phenomenon. Firstly, the hot pressing made the junction among the fibers closer, resulting in a decrease in the pore size and enhancement in the sieving action of the membrane. Moreover, unlike the M1 with an apparent PDA layer (Fig.3), PDA was part of a single fiber in the membrane skeleton of M1', so the pore size became smaller because the fibers became coarser after DA self-polymerization [38]. Secondly, the hydrophilicity of M1 and M1' were markedly improved due to the addition of hydrophilic PDA, thus polar water molecules were allowed to pass through and hydrophobic BSA molecules were trapped on the surface of the fiber membrane. Thirdly, the increase of negative zeta potential of M1 (-3.76±1.19 mV) and M1' (-4.76±0.89 mV) repelled BSA contaminants with the same charge from passing through the membranes, thus obtaining a higher BSA rejection. After the modification of M1 and M1' with nano-zeolite NaX in two different ways, the BSA retention rate of all membranes was still above 90%, which was 30% higher than that

of hot-pressed PAN/PVDF hybrid electrospun nanofiber membranes alone [33]. Except for the above reasons, the adsorption of BSA on the surface of the nano-zeolite NaX was also an important reason. Firstly, the micropores of zeolite NaX (8-9 Å) were tailored to match the side chain size of amino acid residues in BSA, and the exposed amino acids on the protein surface can then extend into the ordered pores on the zeolite NaX surface, leading to specific adsorption [39, 40]. Moreover, acid-base reactions occurred between amino acids of BSAs and hydroxyl groups on the surface of zeolite NaX particles also promoted the retention of BSA [41]. And the slight decrease in BSA rejection was due to two reasons. First, after nano-zeolite NaX modification, the water contact angle of the membranes was further decreased. Although the super-hydrophilicity enabled the formation of better water molecule layers on the membrane surface, it retarded the adsorption of hydrophobic BSA contaminant to a certain extent [25]. Second, the pore size of M2 (0.7244 μm) and M2' (0.6173 μm) was enlarged after modification by nano-zeolite NaX in an alkaline condition, thus the BSA rejection of BSA decreased. However, the difference in BSA rejection between M2 and M3, and between M2' and M3' could be ignored, indicating that the loading environment of nano-zeolite NaX had little effect on the BSA rejection of the membrane.

As far as we know, there are few works of literature on ammonium removal by composite electrospun fiber membranes. In Fig.6c-6d, no $NH_4^+$ removal was obtained for all membranes before modification by nano-zeolite NaX. Interestingly, because of the “double-sided adhesive” effect of the PDA, nano-zeolite NaX was successfully

doped on the membrane whether it was performed in situ or in an aqueous solution. 98±1.9% of $NH_4^+$ removal efficiency was obtained for M2' at the first two minutes due to the ion exchange and surface electrostatic adsorption mechanism [19], then there was a slow decline with prolonging the filtration time. However, the $NH_4^+$ removal efficiency of M3' was only 79±1.6% and the decline rate was fast. It indicated that a few active sites of M3' were available for ammonium exchange because of the aggregation and scab of the nano-zeolite NaX particles (Fig.3). Compared with M2' and M3', the active sites of nano-zeolite NaX on the surface of M2 and M3 were saturated rapidly with the extension of filtration time, as their ammonium adsorption efficiency dropped almost linearly. While the PDA-coated membranes of M2 still exhibited good ammonium removal efficiency at the beginning of filtration. This illustrated that both PDA-coated and blended membranes achieved successful nano-zeolite NaX loading and realized efficient ammonium adsorption. To further verify the adhesion role of PDA in loading nano-zeolite NaX on the electrospun fiber membranes, the PP-H-Z (without PDA coating) and M0'-Z (without inducing DA self-polymerization to form PDA) on $NH_4^+$ removal efficiency was also investigated. As shown in Fig.S3, less than 40% and 30% ammonium removal efficiency were obtained for M0'-Z and PP-H-Z, respectively. This indicated that without PDA layers, the nano-zeolite NaX particles could not be successfully and stably loaded on the fiber film, thus obtaining low ammonium removal efficiency. The inorganic nano-zeolite NaX particles often leads to a lack of compatibility with the organic PVDF/PAN membrane without PDA.

Fig.6e showed that the BSA solution flux of the M1 membrane increased by about 50 L/($m^2$·h) after PDA coating, and it was further enhanced to 210.18±1.5 L/($m^2$·h) after in situ nano-zeolite NaX modification, this was due to the creditable increased hydrophilicity, and the reduced water permeation resistance. The results are similar to the reports by Huang et al. [8] and Zuo et al. [42] investigating PDA-coated membranes. In addition, compared to M1 (0.3365 μm), the increased membrane pore size of M2 (0.7244 μm) also promoted the increase of solution permeability. However, the solution flux of M3 was as low as that of PP at the initial stage of filtration. And the solution flux continuously decreased due to the shedding of nano-zeolite NaX particles, which may increase the filtration resistance. Compared with the low flux of PP (156.78±1.5 L/($m^2$·h)), the solution permeability of M0 was as high as 208.07±0.7 L/($m^2$·h) because of the addition of hydrophilic DA (Fig.6f). And the solution flux of M1' was further increased after DA self-polymerization, which was due to the formation of a good PDA layer on the single fiber surface of PVDF/PAN, making M1' super hydrophilic. After modification by nano-zeolite NaX, the BSA flux of M2' was about 198.17±1.2 L/($m^2$·h), probably due to its super hydrophilicity and large pore size (0.6173 μm). In general, the PDA-blended membrane with in situ nano-zeolite NaX loading strategy proposed in this study was more effective for BSA rejection, $NH_4^+$ removal, and enhancement of solution flux.

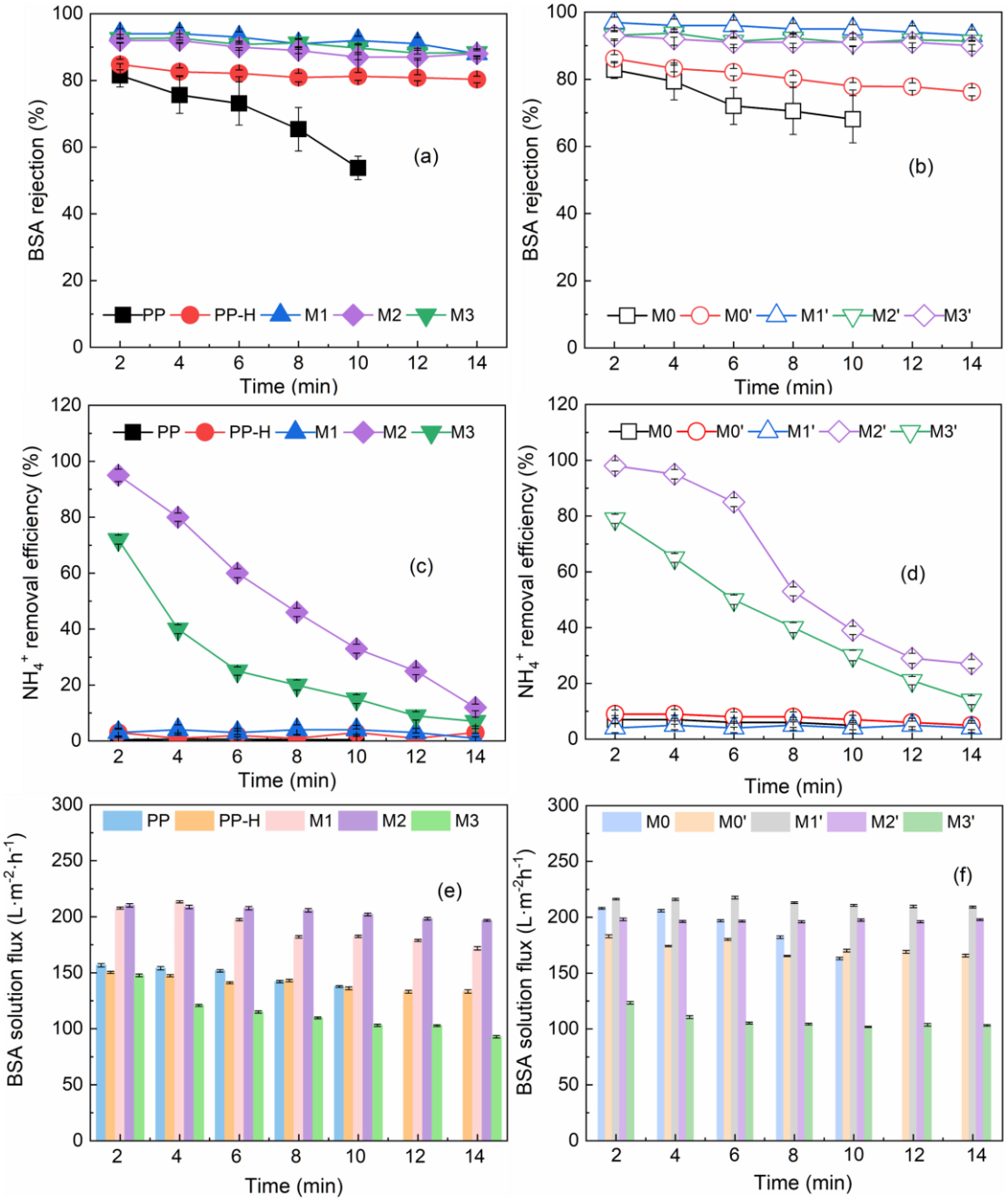


Fig.6 PDA-coated composites (a, c, e) and PDA-blended (b, d, f) composites EMs on the BSA rejection (a, b), $NH_4^+$ removal efficiency (c, d) and BSA solution flux (e, f)

### 3.4 Adsorption kinetics of nano-zeolite NaX-modified composite membranes in static and dynamic ammonium adsorption

Fig.7a showed that in the static adsorption process, the ammonium adsorption rate of the four membranes (M2, M3, M2', and M3') increased dramatically and

reached saturation at 10 min, due to the large specific surface area and abundant available active adsorption sites. While in the dynamic adsorption process, the adsorption equilibrium time of ammonium was extended to 14 min (Fig.7b). This was mainly because, in the static adsorption process, the membranes were cut into small pieces, thus enlarging the contact area. However, the contact area and time were limited in the dynamic process, so the adsorption saturation time was prolonged. Besides, the adsorption capacity of M2 and M2' was all much higher than that of M3 and M3' in the either static or dynamic adsorption process, indicating that in situ loading of nano-zeolite NaX on PDA modified membranes was more efficient for ammonium adsorption. This was because the intact flower-like structures of zeolite NaX nanoparticles were maintained and no agglomeration was observed. Moreover, compared to M2, the higher ammonium adsorption capacity of M2' indicated that loading nano-zeolite NaX by the PDA blending method was more effective than that of PDA coating. This may be because the distribution of PDA in M2' was more uniform after DA self-polymerization, so more phenolic hydroxyl groups and nitrogen-containing groups existed in the fiber surface, resulting in more nano-zeolite NaX particles loading per unit area of the membrane. In addition, more PDA layers can generate more electron transitions and form hydrogen bonds, which had strong adsorption capacity, thus promoting ammonium removal.

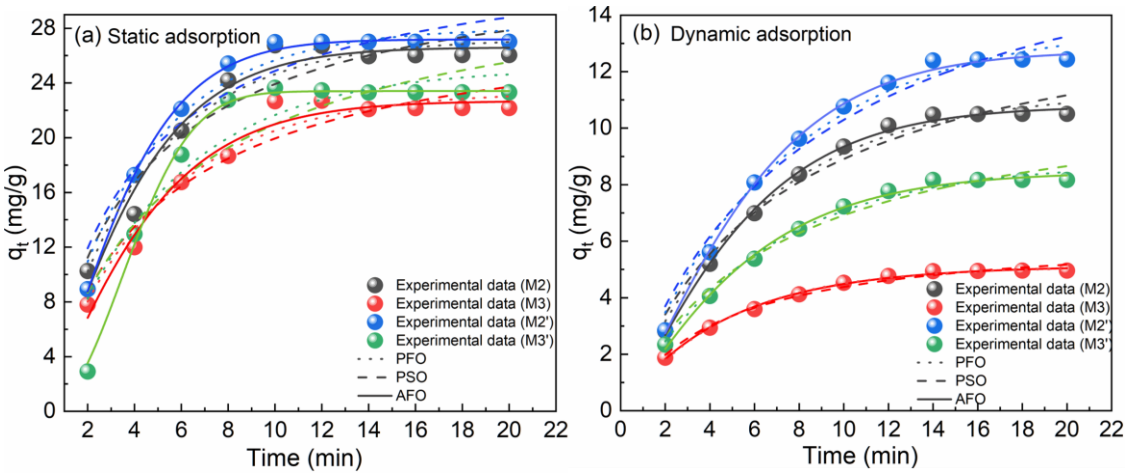


Fig.7 Adsorption kinetics of ammonium in (a) static and (b) dynamic adsorption process by M2, M3, M2', and M3'.

To better quantitatively compare the ammonium adsorption performance of M2, M3, M2', and M3', the nonlinear PFO, PSO, and AFO kinetics models were fitted with the experimental data. As shown in Fig.7 and Table 1, the AFO kinetic model was completely consistent with the experimental data in both static and dynamic ammonium adsorption processes by all nano-zeolite NaX-modified composite membranes. And the maximum experimental adsorption capacity of M2' was 27.02 mg/g, as high as that of the calculated adsorption capacity (27.19 mg/g) in the static adsorption process. Furthermore, the corresponding rate constant $k_{AV}$ (0.1663) of the AFO kinetic model was significantly lower than 1, clearly suggesting the complexity of the adsorption and the characteristics of multiple kinetic stages during the binding procedure of ammonium onto M2'.

Table 1 Kinetics models and their corresponding parameters of ammonium adsorption by M2, M3, M2', and M3'.

| Kinetic models | Kinetic parameters | Membranes | | | |
|---|---|---|---|---|---|
| | | M2 | M3 | M2' | M3' |

| | | | | | | |
|---|---|---|---|---|---|---|
| | | $R^2$ | 0.950 | 0.958 | 0.968 | 0.876 |
| | PFO | $q_e$ (mg/g) | 27.24 | 23.38 | 28.03 | 25.10 |
| | | $k_1$ ($min^{-1}$) | 0.2349 | 0.2101 | 0.2473 | 0.1989 |
| | | $R^2$ | 0.903 | 0.922 | 0.914 | 0.824 |
| Static adsorption | PSO | $q_e$ (mg/g) | 33.33 | 29.26 | 34.19 | 32.57 |
| | | $k_2$ (g/mg·min) | 0.0076 | 0.0073 | 0.0078 | 0.0056 |
| | | $R^2$ | 0.969 | 0.966 | 0.997 | 0.995 |
| | AFO | $q_e$ (mg/g) | 26.61 | 22.69 | 27.19 | 23.41 |
| | | $k_{AV}$ ($min^{-1}$) | 0.2379 | 0.2170 | 0.2521 | 0.2174 |
| | | n | 1.2370 | 1.2292 | 1.3763 | 2.1737 |
| | | $R^2$ | 0.988 | 0.996 | 0.985 | 0.991 |
| | PFO | $q_e$ (mg/g) | 11.32 | 5.10 | 13.68 | 8.78 |
| | | $k_1$ ($min^{-1}$) | 0.1639 | 0.2154 | 0.1464 | 0.1641 |
| | | $R^2$ | 0.970 | 0.984 | 0.968 | 0.975 |
| Dynamic adsorption | PSO | $q_e$ (mg/g) | 14.96 | 6.30 | 18.59 | 11.56 |
| | | $k_2$ (g/mg·min) | 0.0099 | 0.0362 | 0.0067 | 0.0129 |
| | | $R^2$ | 0.997 | 0.995 | 0.998 | 0.995 |
| | AFO | $q_e$ (mg/g) | 10.78 | 5.13 | 12.73 | 8.45 |
| | | $k_{AV}$ ($min^{-1}$) | 0.1781 | 0.2128 | 0.1663 | 0.1753 |
| | | n | 1.2155 | 0.9642 | 1.2859 | 1.1521 |

### 3.6. Effect of PDA and nano-zeolite NaX on the antifouling performance of membrane

To investigate the effect of PDA and nano-zeolite NaX on the antifouling performance of the membranes in detail, the three ratios of FRR, $R_r$, and $R_{ir}$ were calculated. As shown in Fig.8, the $R_{ir}$ of the primitive PP and M0 membrane was as high as 43.63% and 39.18%, and only 56.37% and 60.82% of FRR was obtained, respectively, showing severe membrane fouling after 5 times of filtration. While FRR and $R_{ir}$ of M2' reached 90.62% and 9.38%, indicating that the antifouling performance of PVDF/PAN membrane has been effectively improved with the aid of PDA self-polymerization and in situ loading of nano-zeolite NaX, which was much higher than

the PVDF membranes (FRR: 82.6%) via dopamine-assisted deposition of zwitterionic copolymer [43]. In general, the antifouling performance of the membrane is directly related to the hydrophilicity, roughness, membrane aperture as well as membrane surface charge. As mentioned above, the hydrophilicity of M2 and M2' were significantly increased after modification by PDA and nano-zeolite NaX. And the high hydrophilicity led to the formation of a dense and stable hydration layer on the surface of the membrane, thus slowing down the growth rate of the hydrophobic BSA molecular [44], resulting in a better antifouling performance. In addition, compared to PP and M0, the dramatically high electronegativity of M2 (-23.3±1.3 mV) and M2' (-27.03±2.1 mV) promoted mutual repulsion with negatively charged BSA solution (-8.37±1.7 mV). Moreover, the decreased membrane pore diameter of the M2' diminished the degree of membrane fouling. Besides, the roughness of the membrane is another indicator to evaluate the antifouling performance. Usually, the smoother the surface, the stronger the anti-fouling performance [45]. Because the rough structure of the membrane will increase the contact area between the membrane surface and organic pollutants or bacteria, and easy to produce a “dead zone” with poor hydrodynamic shear stress in crossflow mode, which makes it difficult to wash away the pollutants adhering to or deposited on the membrane, thus aggravating the irreversible pollution [46, 47]. Compared to the membrane surface topography of the PP membrane shown in the three-dimensional image in Fig.S4, the surface of M0 was much smoother, probably due to the addition of DA reducing the peak valleys on the PVDF/PAN membrane. The convex and rough structure of M2 and M2' formed by

anchoring nano-zeolite NaX particles through the hydrogen bonds between polydopamine and nano-zeolite NaX particles, significantly enhanced the roughness of the membrane surface. While the antifouling performance of the M2 and M2' was enhanced. This was because the regular submicron scale surface structure of zeolite NaX particles can improve the shear stress of water flow and generate local turbulence, thus reducing the deposition and adhesion of pollutants on the membrane surface [48]. In addition, it was reported that the randomly oriented nanochannels in the composite membrane can offer much straighter paths for fast water molecule transport [49]. The three-dimensional porous channel structure of zeolite NaX nanoparticles, the interspace between nano-zeolite NaX and PVDF substrate, and the high porosity of fibrous membranes enhanced the permeability, thus reducing the tendency of membrane aperture plugging. Furthermore, the zeolite NaX nanoparticle structure raised on the membrane surface was not easy to be covered by hydrophobic BSA pollutants due to the high electronegativity and hydrophilicity, so the flux recovery ratio was enhanced.

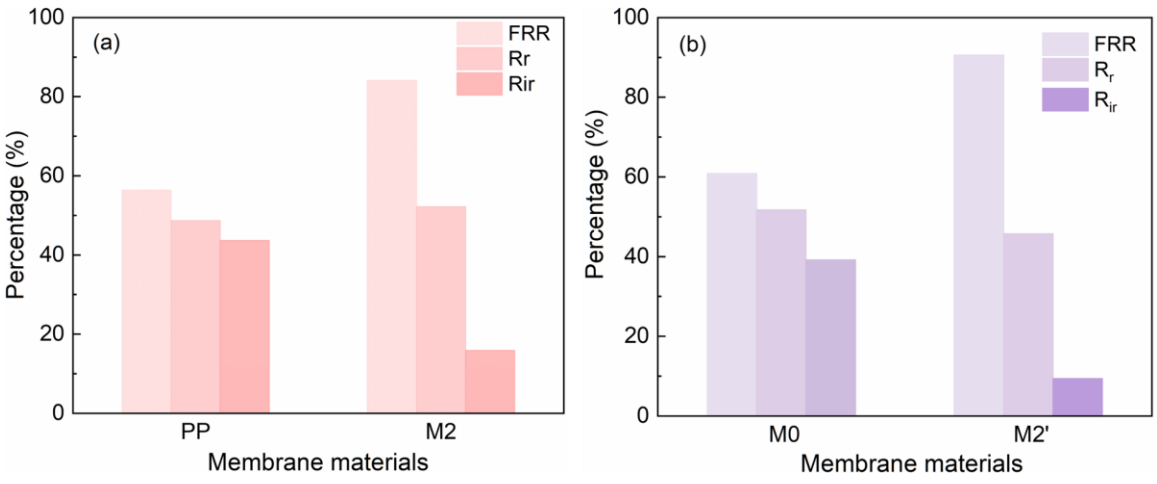


Fig.8 Comparison of FRR, $R_r$ and $R_{ir}$ of M2 and M2' composites EMs under five

cycles of BSA filtration tests.

**3.6 Reusability of** M2 and M2'

After the first filtration, the used M2 and M2' were regenerated according to our reported work [5]. Repeated the above steps for dynamic filtration cycle experiments and the reusability of M2 and M2' were shown in Fig.9. After five cycles, the BSA rejection of M2 and M2' stabilized at about 88% and 90%, respectively. However, their ammonium removal efficiency was a little reduced due to the blockage of the pore channels and the reduction of the basic binding sites. Considering its high BSA rejection and ammonium capacity in five recycles, M2' exhibits the potential to recover carbon and ammonium sources from an aqueous solution and is a promising candidate material for environmental application.

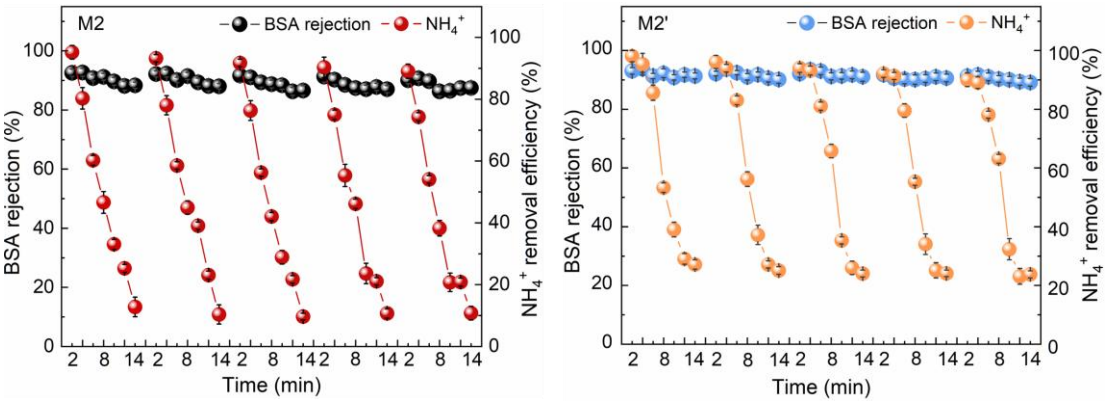


Fig.9 Reusability of M2 and M2' composites EMs on BSA rejection and $NH_4^+$ removal efficiency

**4. Conclusions**

In this study, nano-zeolite NaX particles were successfully loaded on the PDA-coated or PDA-blended electrospun membranes due to the glue effect of PDA. Compared with M3 and M3' obtained by loading nano-zeolite NaX in its aqueous

solution, M2, and M2' achieved by in situ loading of nano-zeolite NaX exhibited higher $NH_4^+$ removal efficiency, BSA retention efficiency, and solution flux due to their super hydrophilic, tailored membrane pore size, high negative potential, and intact nano-zeolite NaX structure. The Avrami fractional-order kinetic model fitted well with the experimental data for all nano-zeolite NaX-modified membranes in static and dynamic adsorption processes. In addition, the antifouling performance of the M2 and M2' was significantly facilitated with excellent flux recover ratio of FRR of 84.11 and 90.62, respectively, due to the enhanced high electronegativity and hydrophilicity after modification by PDA and nano-zeolite NaX particles. Furthermore, M2 and M2' showed excellent stability for high BSA rejection and ammonium adsorption efficiency in five recycles. Our study indicated that M2' obtained in a simple method can act as a cost-effective functional membrane to remove the BSA, and $NH_4^+$ simultaneously at high solution flux in wastewater treatment.

**Acknowledgments**

This research was supported by the Special Research Project of the Shaanxi Provincial Education Department [grant number 22JK0457]; and the National Natural Science Foundation of China [grant number. 52000149].

**References**

[1] X.H. Weifeng Li, Lijian Han, Jingqiao Mao, Mingming Tian, Does urbanization intensify regional water scarcity? Evidence and implications

from a megaregion of China, Journal of Cleaner Production, 244 (2020).

[2] Y.I. Musthafa O. Mavukkandy, Faisal Almarzooqi, Vincenzo Naddeo, Georgios N. Karanikolos, Emad Alhseinat, Fawzi Banat, Shadi W. Hasan,, Synthesis of polydopamine coated tungsten oxide@ poly(vinylidene fluoride-co-hexafluoropropylene) electrospun nanofibers as multifunctional

membranes for water applications, Chemical Engineering Journal 427 427 (2022) 131021.

[3] M. Zarei, Wastewater resources management for energy recovery from circular economy perspective, Water-Energy Nexus, 3 (2020) 170–185.

[4] W.H. Kuo Fang, Fei Peng, Kaijun Wang, Ammonia recovery from concentrated solution by designing novel stacked FCDI cell, Separation and Purification Technology, 250 (2020) 117066.

[5] R.L. Wenyan He, Kuo Fang, Erfu San, Hui Gong b, Kaijun Wang, Fabrication of zeolite NaX-doped electrospun porous fiber membrane for simultaneous ammonium recovery and organic carbon enrichment, Journal of Membrane Science, 603 (2020) 118030.

[6] H.Q.Y. W.W. Li, B.E. Rittmann, Chemistry: Reuse water pollutants, Nature, 528 ( 2015) 29-31.

[7] Soubhagya Nayak, S. Sevda, Urine based bioelectrochemical system: Resources recovery and domestic wastewater treatment prospectives, Bioresource Technology Reports, 20 (2022) 101257.

[8] J.T.A. Liwei Huang, Seetha S.Manickam, Xiaoqiang Jiang, Brian G. Willis, Jeffrey R. McCutcheon, Improved mechanical properties and hydrophilicity of electrospun nanofiber membranes for filtration applications bydopamine modification, Journal of Membrane Science, 460 (2014) 241-249.

[9] N.Z. Fang-fang Ma, Xiao Wei, Jing-hui Yang, Yong Wang, Zuo-wan Zhou, Blend-electrospun poly(vinylidene fluoride)/polydopamine membranes: Self-polymerization of dopamine and the excellent adsorption/separation abilities, Journal of Materials Chemistry A, 5 (2017) 14430-14443.

[10] S.Z. Golshan Moradi, Polycitrate-para-aminobenzoate alumoxane nanoparticles as a novel nanofiller for enhancement performance of electrospun PAN membranes, Separation and Purification Technology, 213 (2019) 224-234.

[11] Nasir Mehranbod, Mohammad Khorram, Samaneh Azizi, N. Khakinezhad, Modification and superhydrophilization of electrospun polyvinylidene fluoride membrane using graphene oxide-chitosan nanostructure and performance evaluation in oil/water separation, Journal of Environmental Chemical Engineering, 9 (2021) 106245.

[12] J.H.S. H. J. Kim Improvement in the mechanical properties of carbon and aramid composites by fiber surface modification using polydopamine Composites Part B Engineering, 160 (2018) 31-36.

[13] Thi Xuan Quynh Nguyen, Shiao-Shing Chen, M.Pasawan, Huy QuangLe, Hau-MingChang, N. CongNguyen, Separation of used automobile oil/water mixture by Nylon 6/ZnO nanoparticles electrospun membrane, Separation and Purification Technology 298 (2022) 121578.

[14] Y.X. Yongqiang Zhao, Chaopu Ti, Jun Shan, Bolun Li, Longlong Xia, and Xiaoyuan Yan, Nitrogen removal capacity of the river network in a high nitrogen loading region, Environmental Science & Technology, 49 (2015) 1427-1435.

[15] W.W.B. W. K. Dodds, J. L. Eitzmann, T. J. Pilger, K. L. Pitts, A. J. Riley, J. T. Schloesser,

D. J. Thornbrugh,, Eutrophication of U.S. Freshwaters: Analysis of Potential Economic Damages, Env iron. Sci. Technol., 43 (2009) 12−19.

[16] X.H. C. Yu, H. Chen, H.C.J. Godfray, J.S. Wright, J.W. Hall, P. Gong, S. Ni, S. Qiao, G. Huang, Y. Xiao, J. Zhang, Z. Feng, X. Ju, P. Ciais, N.C. Stenseth, D.O. Hessen, Z. Sun, L. Yu, W. Cai, H. Fu, X. Huang, C. Zhang, H. Liu, J. Taylor, , Managing nitrogen to restore water quality in China, Nature, 567 (2019) 516-520.

[17] P.V.d.C. Willy Verstraete, Vasileios Diamantis, Maximum use of resources present in domestic ‘‘used water”, Bioresource Technology, 100 (2009) 5537–5545.

[18] M.S. Sri Abirami Saraswathi, Divya, K., Rana, D., Nagendran, A., Metal-organic frameworks based membranes for water treatment applications. In: Nano-Enabled Technologies for Water Remediation, Kaleekkal, N. J., Mural, P. K. S., Vigneswaran, S. (Eds.), Elsevier, Amsterdam, Netherlands, Ch. 11, pp. 335-354.

[19] H.G. Wenyan He, Kuo Fang, Fei Peng, Kaijun Wang,, Revealing the effect of preparation parameters on zeolite adsorption performance for low and medium concentrations of ammonium, Journal of Environmental Sciences, 85 (2019) 177-188.

[20] N.Z. Y.F. Deng, T. Huang, Y.Z. Lei, Y. Wang,, Constructing tubular/porous structures toward highly efficient oil/water separation in electrospun stereocomplex polylactide fibers via coaxial electrospinning technology, Applied Surface Science, 573 (2022) 151619.

[21] Y.H. Siyi Xu, Cheng Zhou, Jianxi Li, Liguo Shen, Hongjun Lin,, A biobased flame retardant towards improvement of flame retardancy and mechanical property of ethylene vinyl acetate, Chinese Chemical Letters, 34 (2023) 107202.

[22] S.M.D. Haeshin Lee, William M. Miller, Phillip B. Messersmith, Mussel-Inspired Surface

Chemistry for Multifunctional Coatings, Science, 318 (2007) 426–430.

[23] L.Z. J. Jiang, B. Zhu, Y. Xu,, Surface characteristics of a self-polymerized dopamine coating deposited on hydrophobic polymer films, Langmuir, 27 (2011) 14180–14187.

[24] Y.W. Y. N. Gao, T. N. Yue, Y.X. Weng, M. Wang,, Multifunctional cotton non-woven fabrics coated with silver nanoparticles and polymers for antibacterial, superhydrophobic and high performance microwave shielding, Journal of Colloid and Interface Science, 582 (2021) 112-123.

[25] Z.X.W. L. Shao, Y.L. Zhang, Z. X. Jiang, Y.Y. Liu,, A facile strategy to enhance PVDF ultrafiltration membrane performance via self-polymerized polydopamine followed by hydrolysis of ammonium fluotitanate, Journal ofMembraneScience, 461 (2014) 10-21.

[26] K.B. D. RANA, S. N. BHATTACHARYYA, B. M. MANDAL, Miscibility of Poly(styrene-co-butyl acrylate) with Poly(ethylmethacrylate): Existence of Both UCST and LCST, J. Polym. Sci. Polym. Phys. Edit. 38 (3) (2000) 38 (2000) 369–375.

[27] B.M.M. D. Rana, S. N. Bhattacharyya, Analogue Calorimetric Studies of Blends of Poly(vinyl ester)s and Polyacrylates, Macromolecules, 29 (1996) 1579-1583.

[28] B.M.M. D. Rana, S. N. Bhattacharyya Miscibility and phase diagrams of poly ( phenyl acrylate) and poly (styrene-co□acrylonitrile) blends, Polymer, 34 (1993).

[29] B.M.M. D. Rana, S. N. Bhattacharyya, Analogue calorimetry of polymer blends: oly(styrene-co-acrylonitrile) and poly(phenyl acrylate) or poly(vinyl benzoate) Polymer 37 (1996) 2439.

[30] R.D. S.A.S. A, D. Kumar, N.A. A. S, Fabrication of anti-fouling PVDF nanocomposite membranes using manganese dioxide nanospheres with tailored morphology, hydrophilicity

and permeation, New Journal of Chemistry, 42 (2018) 15803-15810.

[31] H.X. Yu, L. Gu, S.F. Wu, G.X. Dong, X.B. Qiao, K. Zhang, X.Y. Lu, H.F. Wen, D.F. Zhang, Hydrothermal carbon nanospheres assisted-fabrication of PVDF ultrafiltration membranes with improved hydrophilicity and antifouling performance, Separation and Purification Technology, 247 (2020) 116889.

[32] H.J. FuSheng Pan, ShiZhang Qiao, ZhongYi Jiang, JingTao Wang, BaoYi Wang, YuRong Zhong, Bioinspired fabrication of high performance composite membranes with ultrathin defect-free skin layer, Journal of Membrane Science 341 (2009) 279–285.

[33] R.S. ZhaoWang, Caitlin Crandall, Todd J. Menkhaus, Hao Fong,, Hot-pressed PAN/PVDF hybrid electrospun nanofiber membranes for ultrafiltration, Journal of Membrane Science, 611 (2020) 118327.

[34] G.-D.C. Bo Lin, Fu-An He, Ying Li, Ying Yang, Bo Shi, Feng-Ru Feng, Song-Yun Chen, Kwok-Ho Lam,, Preparation of MWCNTs/PVDF composites with high-content β form crystalline of PVDF and enhanced dielectric constant by electrospinning-hot pressing method, Diamond and Related Materials, 131 (2023) 109556.

[35] J.L. Jiachen Huang, Xiangrong Chen, Shichao Feng, Yinhua Wan, New insights into effect of alkaline cleaning on fouling behavior of polyamide nanofiltration membrane for wastewater treatment, Science of the Total Environment, 780 (2021) 14663.

[36] X.-X.K. Bing Li, Zhi-Hua Yuan, Lu-Bin Zhong, Quan-Bao Zhao, Yu-Ming Zheng, High performance electrospun thin-film composite forward osmosis membrane by tailoring polyamide active layer with polydopamine interlayer for desulfulrization wastewater desalination, Desalination 534 (2022) 115781.

[37] S.R.N. Fatemeh Ebrahimi, Abdolah Omrani, Fabrication of hydrophilic hierarchical PAN/SiO2 nanofibers by electrospray assisted electrospinning for efficient removal of cationic dyes, Environmental Technology & Innovation 25 (2022) 102258.

[38] Xuefen Wang, Benjamin S Hsiao, Electrospun nanofiber membranes, Current Opinion in Chemical Engineering, 12 (2016) 62–81.

[39] John E. Krohn, M. Tsapatsis, Amino Acid Adsorption on Zeolite β, Langmuir, 21 (2005) 8743-8750.

[40] Kai Stu¨ckenschneider, Juliane Merz, Felix Hanke, Piotr Rozyczko, Victor Milman, Gerhard Schembecker, Amino-acid adsorption in MFI-type zeolites enabled by the pH-dependent ability to displace water, J. Phys. Chem. C, 117 (2013) 18927-18935.

[41] Adalgisa Tavolaro, Palmira Tavolaro, Enrico Drioli, Zeolite inorganic supports for BSA immobilization: Comparative study of several zeolite crystals and composite membranes, Colloids and Surfaces B: Biointerfaces, 55 (2007) 67–76.

[42] Zuo, Ji-Hao, Cheng, Peng, Chen, Xing-Fan, Yan, Xi, Guo, Ya-Jun, Ultrahigh flux of polydopamine-coated PVDF membranes quenched in air via thermally induced phase separation for oil/water emulsion separation, Separation & Purification Technology, (2018).

[43] Y.F.W. Z.Q. Liu, F.X. Lan, G.Y. Xie, M.C. Zhang, C.P. Ma, J.B. Jia,, Improvement of permeability and antifouling performance of PVDF membranes via dopamine-assisted deposition of zwitterionic copolymer, Colloids and Surfaces A: Physicochemical and Engineering Aspects, 656 (2023) 130505.

[44] S.S.M. V. Vatanpour, L. Rajabi, S. Zinadini, A. A. Derakhshan,, Boehmite nanoparticles as a new nanofiller for preparation of antifouling mixed matrix membranes, Journal of

Membrane Science, 401–402 (2012) 132–143.

[45] D.R. M.S.S.A. Saraswathi, P. Vijayakumar, S. Alwarappan, A. Nagendran, , Tailored PVDF nanocomposite membranes using exfoliated MoS2 nanosheets for improved permeation and antifouling performance, New J. Chem. , 41 (2017) 14315-14324.

[46] D.P. C. N. Shang, S. Zhang, Understanding the Roughness–Fouling Relationship in Reverse Osmosis: Mechanism and Implications, Environ. Sci. Technol, 54 (2020) 5288–5296.

[47] M. F. Wu, M. J. Zhang, L. G. Shen, X. H. Wang, D. Ying, H. J. Lin, R. J. Li, Y. C. Xu, H. C. Hong, High propensity of membrane fouling and the underlying mechanisms in a membrane bioreactor during occurrence of sludge bulking Water Research, 229 (2023) 119456.

[48] S. H. Maruf, A. R. Greenberg, J. Pellegrino, Y. F. Ding, Fabrication and characterization of a surface-patterned thin film composite membrane Journal of Membrane Science, 452 (2014) 11-19.

[49] Y. C. Xu, W. T. Zhang, Z. W. Li, L. G. Shen, R. J. Li, M. J. Zhang, Y. Jiao, H. J. Lin, C. Y. Y. Tang, Enhanced water permeability in nanofiltration membranes using 3D accordion-like MXene particles with random orientation of 2D nanochannels, Journal of Materials Chemistry A, 10 (2022) 16430.